

VALIDATION OF IN-TUNNEL HIGH LIFT COMPUTATIONS

J.-C. Courty^{*}, T. Delille[†]
DASSAULT-AVIATION
78 Quai Marcel Dassault 92210 Saint-Cloud
France

OVERVIEW

During EUROLIFT I project some questions were left unanswered to understand the differences between computations and wind tunnel results in high lift configurations. To take into account the walls and peniche effects the experimental results are corrected with some laws of correction. Usually the computations are made in free flight conditions and compared with corrected experimental results. One of the aims of EUROLIFT II project co-financed from the EC was to validate high lift computations without considering laws of correction used in wind tunnel tests. Therefore we made computations with walls and peniche and compared numerical results with uncorrected experimental results.

The test case studied was the LSWT wind tunnel where some experiments were made on the KH3Y model in high lift configuration. The first step of the study was to create the mesh with walls and peniche. Then we did computations with the in-house unstructured finite element Navier-Stokes code AETHER with two different turbulent models K-EPSILON SST and K-KL EARSMS. The computations were made for three angles of attack (one in the linear part of the polar, one for maximal angle of attack and one in the stall zone of the polar).

The results of the in-tunnel computations are in pretty good agreement with the experimental wind tunnel results.

NOMENCLATURE

P_0	= Static Pressure measured at the entrance of wind tunnel
V_0	= Freestream Velocity measured at the entrance of wind tunnel
T_0	= Static Temperature measured at the entrance of wind tunnel
Mach	= Mach Number measured at the entrance of wind tunnel
Re	= Reynolds Number
δ	= Boundary Layer Thickness
CL	= Lift Coefficient
CD	= Drag Coefficient
CM_{25}	= Pitching Momentum Coefficient
α	= Angle of attack
Kp	= Wall Static Pressure Coefficient
Hi	= Incompressible boundary layer shape parameter
Beta	= Boundary layer shear angle

k- ϵ SST	= Standard k- ϵ in two layer formulation combined with Shear Stress Transport
k-kl EARSMS	= k-kl combined with EARSMS (Explicit Algebraic Reynolds Stress Model)
DVi	= Section i on the KH3Y model
Lref	= Reference Chord
Sref	= Reference Area

INTRODUCTION

During EUROLIFT II project the effects of the model deformation and of the geometrical model installation were assessed to understand the differences between free flight computations and corrected wind tunnel results (the results are described in [3]). The objective of the work described in this paper is to perform RANS computations on unstructured mesh including wind tunnel walls and peniche and compare them to the uncorrected wind tunnel results. This comparison will allow us to validate the computations in high lift configuration. We have performed calculations for three uncorrected angles of attack: α_1 , α_2 and α_3 . The first one belongs to linear area, the second is the maximal incidence and the third one belongs to the post stall area.

1. CONDITIONS OF THE STUDY

The study is based on wind tunnel tests made during EUROLIFT I project in LSWT (Low Speed Wind Tunnel) in Bremen. The model KH3Y was used for the experiments. This part presents the wind tunnel tests conditions and the principle of the study. In EUROLIFT II project a similar study was accomplished for the wind tunnel ETW (see reference [4]).

1.1. Description of wind tunnel LSWT

The model used is the KH3Y model with a fuselage of Airbus A340-200 type (scale 1/19) and a high-lift wing with H8Y-geometry (scale 1/29) with an extended flap.

The wind tunnel consists of a 3D nozzle, a closed test section, an open main circuit with the driving impeller (Eiffel type) and diffuser. The test section has a cross section of 2.1m \times 2.1m and a length of 4.45m. The figure 1 shows a global view of wind tunnel.

^{*} Head, Advanced Aerodynamics, 78 quai Marcel Dassault, 92210 Saint-Cloud

[†] Senior Scientist, Advanced Aerodynamics, 78 quai Marcel Dassault 92210 Saint-Cloud

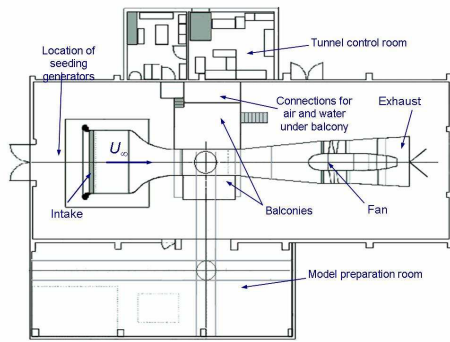


FIG 1. Global view of the wind tunnel LSWT (AIRBUS-Bremen)

The half-model is mounted on the wind tunnel ceiling as shown in the figure 2. A boundary layer plate (peniche) was inserted between half-fuselage and tunnel top wall and fixed to the tunnel wall turntable. Between the peniche and the half-fuselage a labyrinth seal was installed. The height of the peniche including the labyrinth seal is 95mm. The wing is equipped with pressure measurement instrumentation, distributed along eleven spanwise sections DV01 to DV11 as sketched in figure 3.

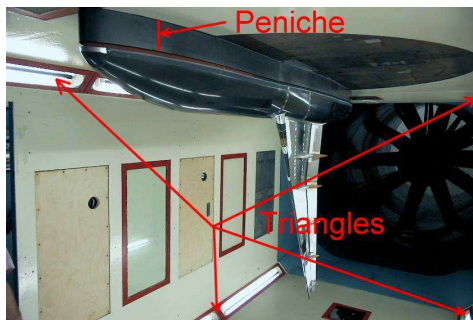


FIG 2. wind tunnel half-model KH3Y mounted in LSWT

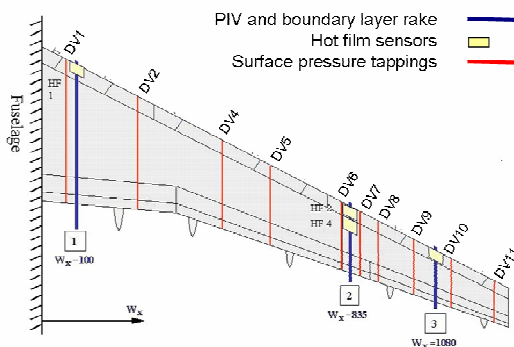


FIG 3. Spanwise location of the sectional pressure taps (DV)

1.2. Description of wind tunnel tests

The test case used in this study is TC211. It corresponds to a take-off configuration that is the slat deflected to 20° and the flap to 22°. The general conditions are:

- Mach = 0.174
- Re Number = 1.34E+06

$$- P_0 = 1006.3 \text{ hPa}; T_0 = 25.8 \text{ }^\circ\text{C}$$

The values of Reynolds number, static pressure and temperature evolve with the angle of attack. The values presented above are mean values.

The lift (CL), drag (CD) and pitching momentum (CM_{25}) coefficients are expressed in the aerodynamic reference frame (Za and Xa axis of figure 4) .

The reference area is $S_{ref}=0.41913 \text{ m}^2$, the reference chord is $L_{ref}=347.09 \text{ mm}$ and the Moment reference is the green point presented in the figure 4 below. The half wing span is 1400.0 mm and the fuselage length is 3077 mm.

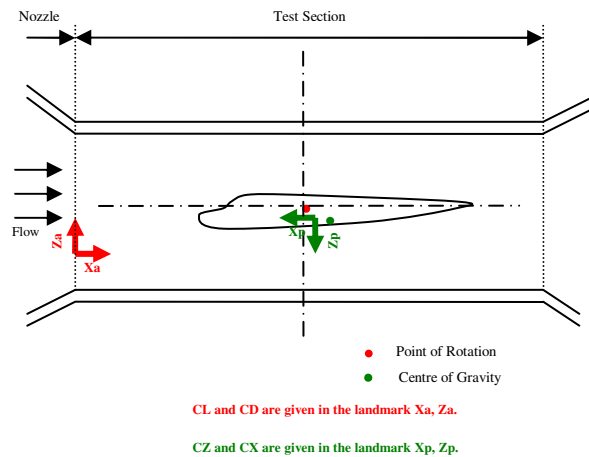


FIG 4. sketch of the model in the wind tunnel LSWT

2. PRINCIPLE OF THE IN-TUNNEL COMPUTATIONS

The in-tunnel computations take into account peniche and wind tunnel walls. This type of simulation requires some specific boundary conditions.

2.1. The boundary conditions

The in-tunnel computations will allow us to assess our numerical method (type of turbulence model, boundary conditions type...) for high lift configuration in confined surrounding. If the numerical results are consistent with the uncorrected experimental results the numerical simulation method will be validated.

The walls and peniche have been considered in the geometry. We needed to increase the length of the tunnel at the entrance and at the exit to stabilise the conditions (pressure, temperature...). The figure 5 represents the boundary conditions for this type of computations.

At the wind tunnel entrance are imposed the density and velocity that is the flow rate. At the exit is imposed the static pressure. Due to the extra tunnel lengths we had to adjust the static pressure at the exit to obtain the wind tunnel conditions (Mach number and static pressure) at the test section entry.

The reference [1] contains some data that concern the measuring of the boundary layers thickness on wind

tunnel walls in the same conditions of pressure and velocity without presence of the model. We have assumed that this one does not influence a lot this measurement. At the entrance we have imposed a boundary layers thickness and adjusted the value to obtain the measured boundary layers thickness at the test section.

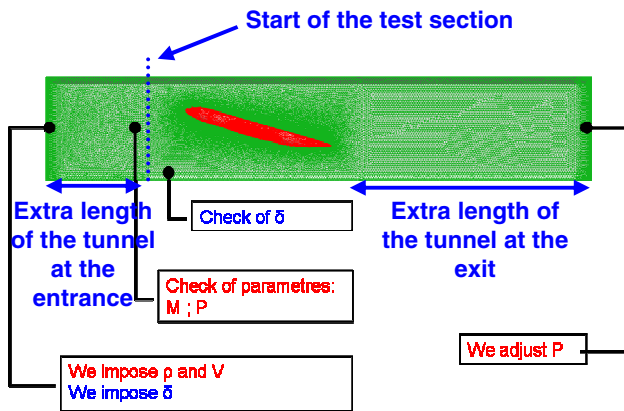


FIG 5. Boundary conditions for the in-tunnel computations

2.2. Description of the meshes

We will first present the skin meshes of the KH3Y model and of the wind tunnel. Then we will present the 3D mesh used for computations with walls and peniche.

The KH3Y model skin mesh includes 57 463 nodes. The fuselage surface grid is unstructured and wing's one is like a structured mesh (but not written as a structured one) in order to have a better prediction. Grid refinement has been introduced at the wing tip and at the leading edges of the slat, main wing and flap (see figure 6).

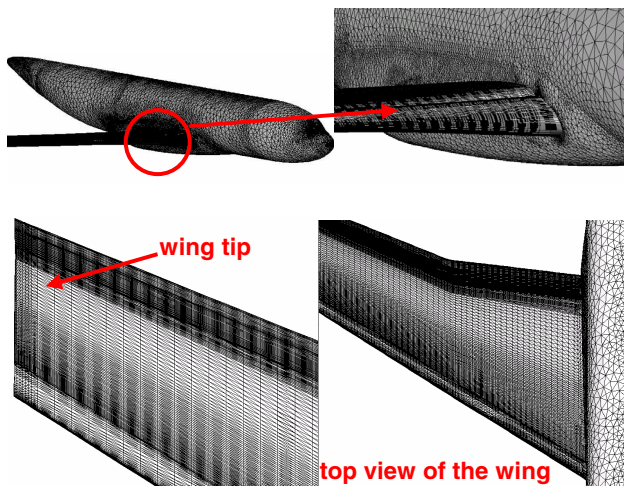


FIG 6. Different views of the model KH3Y skin mesh

We have begun to build a surface grid for the real test section with the model and peniche inside. Then we have added 2 meters of tunnel before the test section in order to permit boundary layer establishment. And we have added 4.5 meters of tunnel behind the test section to let pressure develops (see figure 7).

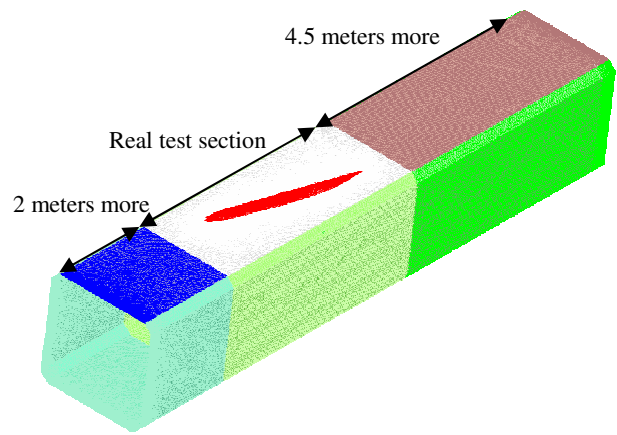


FIG 7. Skin mesh of the model in wind tunnel LSWT with extra parts

The figures below present some views of the wind tunnel mesh. The number of nodes is 95 297.

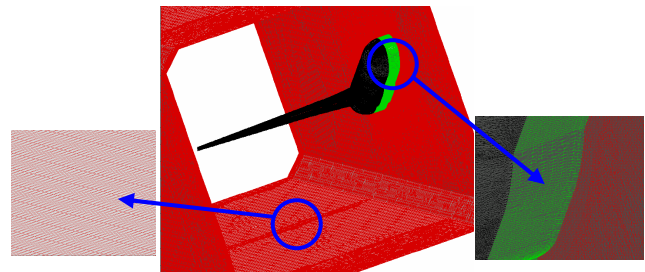


FIG 8. Different views of the model, wind tunnel walls and peniche skin mesh

For the 3D mesh we raised 64 layers from skin with frontal method with a first layer size of $3 \mu\text{m}$ on the model and $5 \mu\text{m}$ on the walls. A viscous grid was generated for the entire wind tunnel. The geometric ratio used for mesh thickening is 1.15. Then we used a Delaunay method to fill the middle of wind tunnel (isotropic 3D mesh). Finally the total number of nodes is 6 827 173.

The figure 9 shows the mesh around the wing including the raising of layers (Frontal method) and the figure 10 presents the mesh in a wind tunnel part without the model.

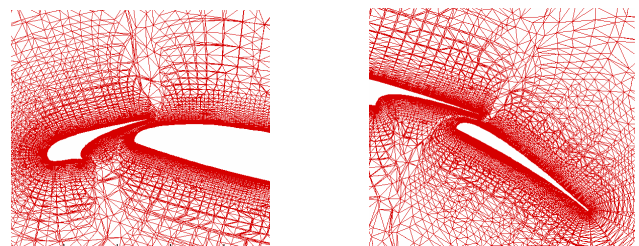


FIG 9. 3D mesh on the wing

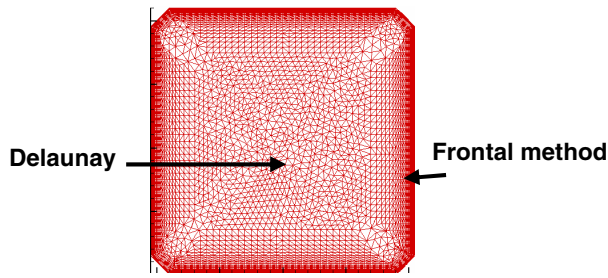


FIG 10. 3D mesh in the wind tunnel

3. IN-TUNNEL NUMERICAL RESULTS

In this part we will first present the realisation of the computations. Then we will show the global numerical results compared to direct wind tunnel results. At the end of this part we will analyse the results with different visualisations.

3.1. Realisation of the computations

The computations were realised for three angles of attack:

- α_1 = angle in the linear part of the wind tunnel polar curve
- α_2 = maximal angle of attack
- α_3 = angle in the post-stall area of the wind tunnel polar curve.

For each case the wind tunnel conditions are given in table 1.

α	Re	Mach	V0 (m/s)	T0 (°C)	P0 (hPa)
α_1	1,310E+09	0,174	60,1	25,65	982,96
α_2	1,309E+09	0,174	60,1	25,76	982,86
α_3	1,306E+09	0,174	60,1	26,09	982,99

TAB 1. Wind tunnel conditions for each angle of attack

As explained in paragraph 2.1 we had to adapt the numerical boundary conditions to get the wind tunnel conditions at the test section.

First we imposed velocity and density (as measured in experiment) in numerical entry plan. Then we adjusted the exit plan pressure in order to obtain the entry test section experimental values expressed in table 1 (figure 5).

Secondly we adjusted the boundary layer thickness at the numerical entry plan. Actually thicker is the boundary layer more important is the blocking effect which influences the results. We have imposed different boundary layer thicknesses at the numerical entry plan until we obtained the experimental value at the measurement location (1 meter after the test section entry). Figure 11 shows the numerical boundary layer thickness evolution on the wind tunnel floor.

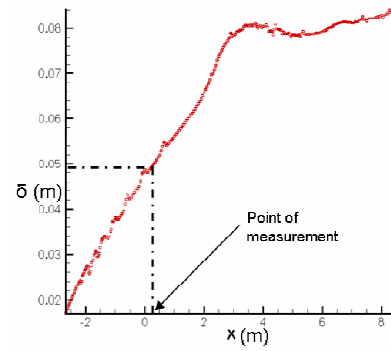


FIG 11. Numerical Evolution of boundary layer thickness on wind tunnel floor

Figure 12 shows the numerical convergence for two angles of attack. We can see that the convergence is regular and obtained for 9000 iterations.

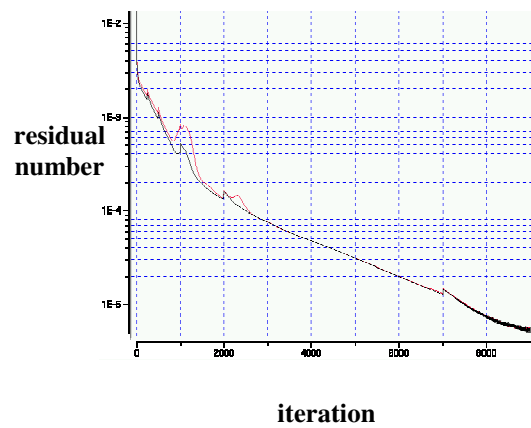


FIG 12. Convergence history for α_1 (black curve) and α_2 (red curve)

3.2. Global numerical results and comparison with wind tunnel tests

The in-tunnel numerical results will be compared to the experimental results. We will compare the polar curves, the K_p (pressure coefficient) distribution and visualisations of different parameters on model skin. In the table 2 are presented for each angle of attack and different turbulence models the global coefficients CL , CD and CM_{25} (Lift, Drag and pitching Moment) compared to the wind tunnel results. The reference area is $S_{ref}=0.41913 \text{ m}^2$ and the reference chord is $L_{ref}=347.09 \text{ mm}$. CD values were obtained with a software (FFD71 developed by ONERA) which is able to subtract the spurious drag component.

α	Turbulence Model	$CL_{exp} - CL_{num}$	$CD_{num} - CD_{exp}$	$CM_{25num} - CM_{25exp}$	$L/D_{exp} - L/D_{num}$
α_1	k- ϵ SST	0.0034	0.0126	0.0002	1.2
α_2	k- ϵ SST	0.0366	0.0112	-0.0077	0.9
α_3	k- ϵ SST	0.5508	0.0696	-0.2226	4.9
α_3	k-kl EARSM	0.0925	0.0269	0.0563	1.7

TAB 2. Global in-tunnel numerical results

The in-tunnel computations give good agreement with

uncorrected experimental results above all in the linear part of the polar until the maximal lift coefficient value. It appears some differences between both turbulence models in the stall zone as observed in the in-tunnel computations. The k-kl EARSM model give better results in that zone than the k-ε SST model.

Below we present different curves that compare global coefficients deduced from computations and experiments: CL function of uncorrected angle of attack (figure 13), polar curve (figure 14) and CM₂₅ function of uncorrected angle of attack (figure 15).

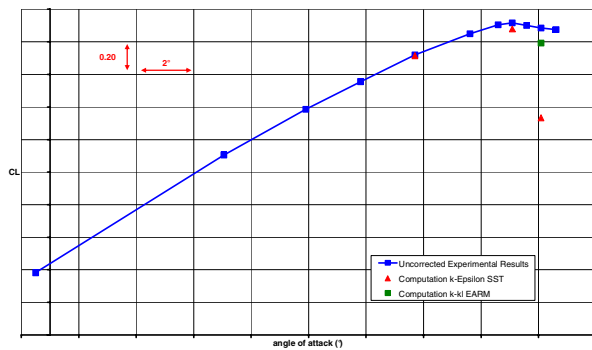


FIG 13. Comparison between Lift coefficients function of uncorrected angle of attack deduced from in-tunnel computations and uncorrected wind tunnel results

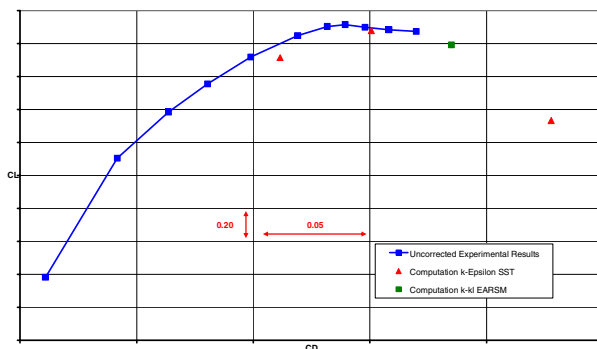


FIG 14. Comparison between the polar curves deduced from in-tunnel computations and uncorrected wind tunnel results

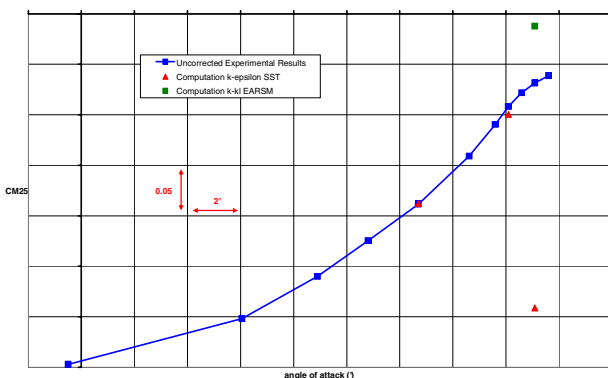


FIG 15. Comparison between the momentum curves deduced from in-tunnel computations and uncorrected wind tunnel results

The different graphics confirm the good agreement between the numerical and experimental results until the maximum lift coefficient. After the maximum angle of attack the k-ε SST turbulence model seems to be too much pessimistic compared to the k-kl EARSM turbulence model.

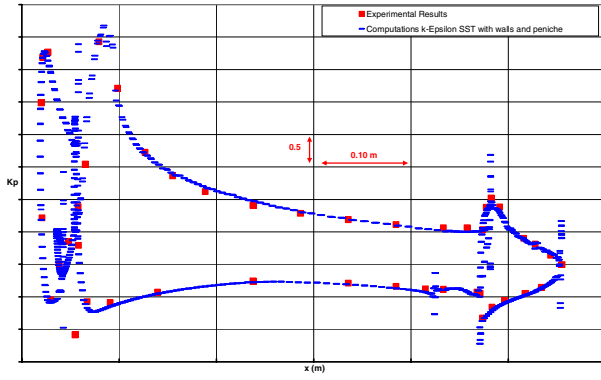
In the next part we will compare the Kp distribution on different sections and some skin variables visualisations on the model.

3.3. Analysis of the results and comparison between the different turbulence models

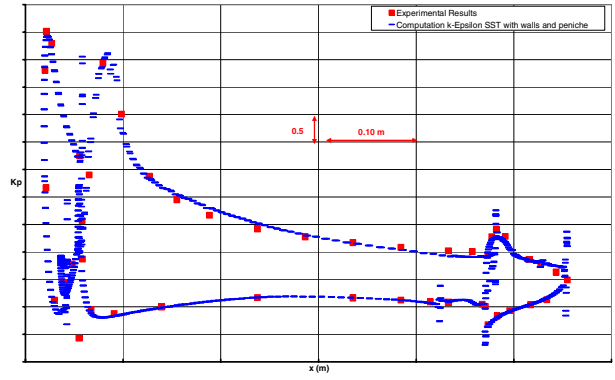
The Kp distribution has been studied on the KH3Y model sections DV1, DV6 and DV10 (figure 3) for three angles of attack and for the different turbulence models (for uncorrected angle of attack equal to α_3). The figures below present the comparison between the Kp distribution given by computations and experimental results for each angle of attack. The variable "x" is the abscissa expressed in meter on the section DV1, DV6 or DV10.

For α_1 we have really good agreement as shown in figure 16. We have just lower suction peak on the flap for the section DV10 which is the closest to the wing tip.

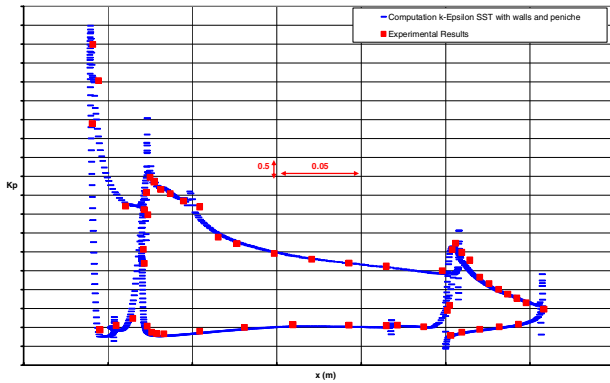
For α_2 (figure 17) we have still good agreement on the windward side. But we notice some differences for the leeward side. The suction peak is lower for the computations than for experiments particularly at the leading edge of the flap. We do not catch completely the acceleration of the flow due to perhaps the wake of the main body. The grid has perhaps to be refined in this area. Closer we are to the wing tip, lower is the suction peak at the flap leading edge in the computations.



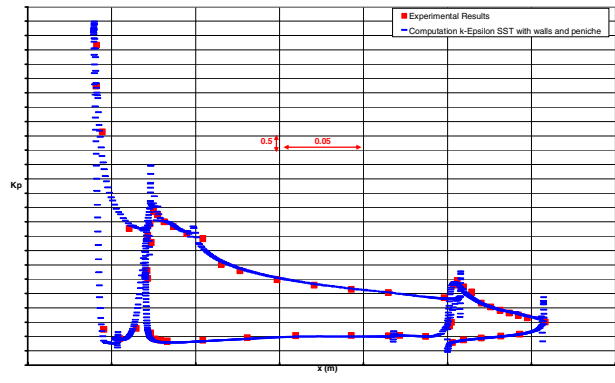
DV1



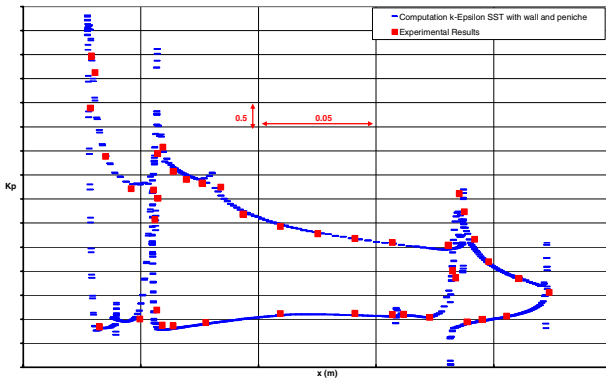
DV1



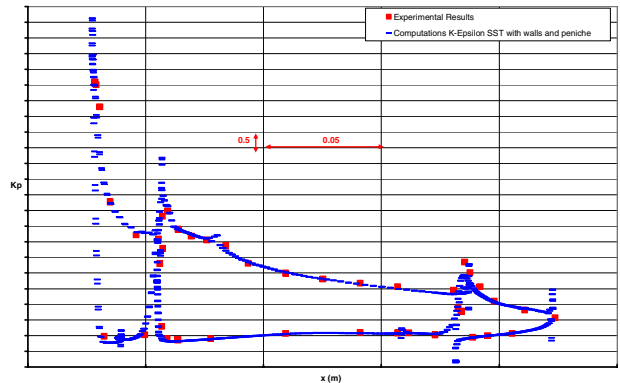
DV6



DV6



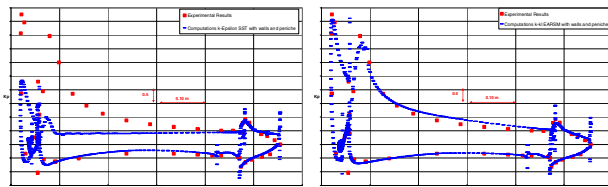
DV10



DV10

FIG 16. Comparison of the Kp distribution between the in-tunnel computations and experimental results for α_1

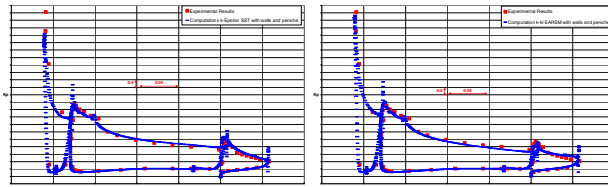
FIG 17. Comparison of the Kp distribution between the in-tunnel computations and experimental results for α_2



k-ε SST

k-kl EARS

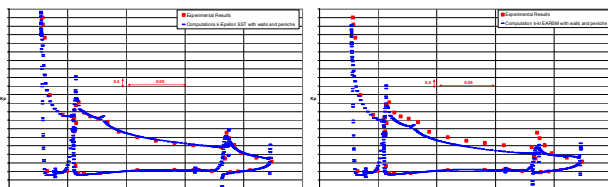
DV1



k-ε SST

k-kl EARS

DV6



k-ε SST

k-kl EARS

DV10

FIG 18. Comparison of the Kp distribution between the in-tunnel computations and experimental results for α_3 for k-ε SST and k-kl EARS turbulence models

For α_3 (figure 18) we get good agreement with the k-ε SST model for the sections DV6 and DV10. But the computations present a big separation area on the main body for the inboard part of the wing (section DV1). The size of the separation area is not so big on the experimental results and suction peak is much higher.

The k-kl EARS results are better for the section DV1 which do not present anymore the separation area on the main body. But the results are not so good for the sections DV6 and DV10 than the k-ε SST model, above all on the flap.

We can compare different angles of attack and different turbulence models with some skin visualisations. Analysis is performed for the following parameters:

- Kp : pressure coefficient

- Hi : when this variable is higher than 2.4 we can consider the boundary layer separated. It characterizes the 2D separations of the boundary layer.

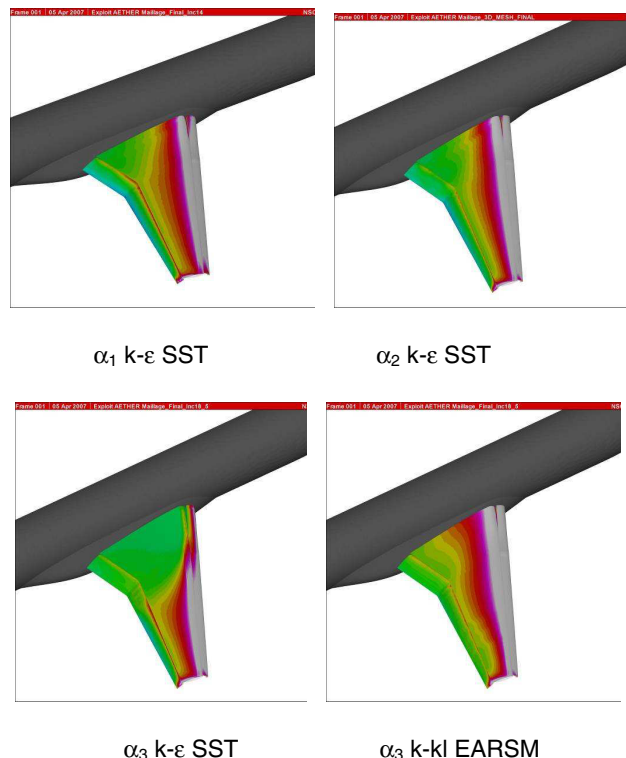
- Beta : when this variable is higher than 45° or lower than -45° we can consider the boundary layer separated. It characterizes the separation of boundary layer due to shear forces. The visualisations of Beta will be associated with skin friction lines.

Figure 19 presents the Kp distribution on the wing. Figure 20 presents the visualisations of separation areas with the variable Hi. Figure 21 shows the beta distribution with skin friction lines on wing.

By observing the evolution of the k-ε SST Kp distribution we can notice the development of a big separation area in the inboard part of the wing with the angle of attack. The loss of lift after α_2 seems to be due to this separation. This fact is confirmed with the other types of visualisations (Hi, Beta and skin friction lines). With k-ε SST model the flap does not seem to be separated.

At α_3 the separation close to the fuselage does not present a so big development for k-kl EARS model than for k-ε SST. But we observe little separation areas close to the wing tip on the slat, the trailing edge of the main body and the flap. Globally we obtain with this kind of turbulence model a higher lift level.

The k-ε SST model seems to be correct for the linear part of the polar but too pessimistic for the stall zone. It amplifies the size of the vortex located close to the fuselage.



α_1 k-ε SST

α_2 k-ε SST

α_3 k-ε SST

α_3 k-kl EARS

FIG 19. Kp visualisations of in-tunnel computations for different uncorrected angles of attack and different turbulence models

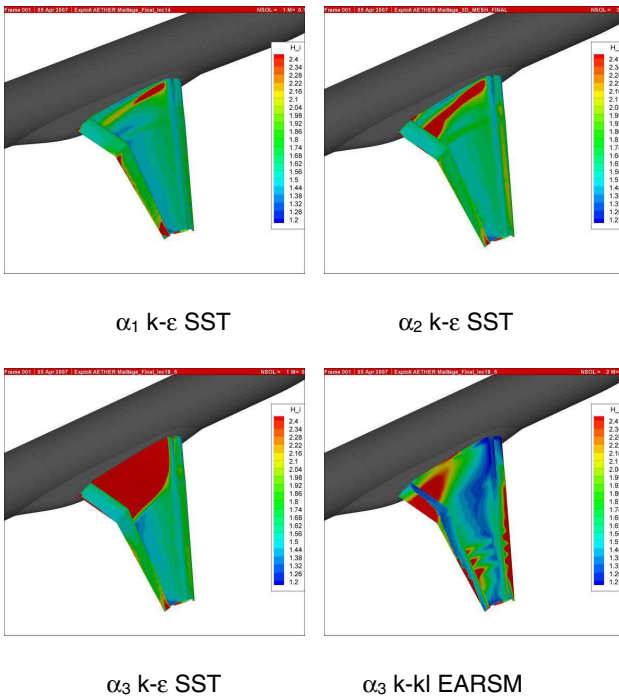


FIG 20. Hi visualisations of in-tunnel computations for different uncorrected angles of attack and different turbulence models

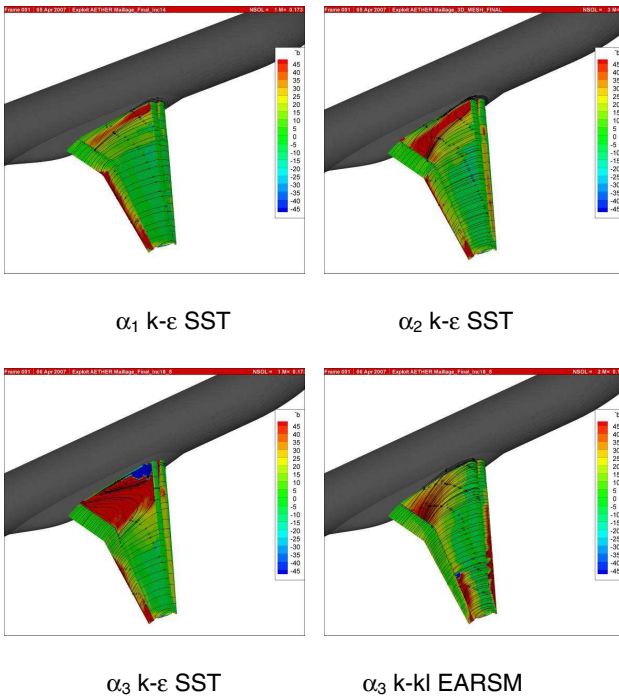


FIG 21. Beta visualisations with skin friction line of in-tunnel computations for different uncorrected angles of attack and different turbulence models

CONCLUSION

During the study we have validated our Navier-Stokes solver AETHER for high lift configurations by comparing in-tunnel computations with direct wind tunnel tests results. We have tested two turbulence models : k- ϵ SST and k-k1 EARSM. It appears that both models give good results until the maximal angle of attack; the k-k1 EARSM model giving better results in the stall area.

ACKNOWLEDGMENTS

The research work discussed in the paper was performed under the European research contract G4RD-CT-1999-00072 in the project EUROLIFT as part of the 5th framework programme, and under contract AST2-2004-502896 in the project EUROLIFT II as part of the 6th framework programme. The authors would like to thank the European Commission for co-funding this research activity as well as all involved EUROLIFT partner.

REFERENCES

- [1] "WX 03-25-4 Extract of wind tunnel calibration - Measuring of the boundary layer", S. Wyrembek, Airbus References.
- [2] EUROLIFT Technical Report N° D3.2-6, "Model Description KH3Y (DLR F11) with new flap system", W. Puffert-Meißner, DLR-Institute of Aerodynamics and Flow Technology.
- [3] "Geometrical Model Installation and Deformation Effects in the European project EUROLIFT II", J. van der Burg, et.al., AIAA-2007-4297, 2007.
- [4] "Numerical Validation of a Half Model High Lift Configuration in a Wind Tunnel", P. Eliasson, AIAA 2007-262, 2007.